Ecological Applications, 7(1), 1997, pp. 3–21

USE OF USGS-PROVIDED DATA TO IMPROVE WEATHER AND CLIMATE SIMULATIONS

R. A. PIELKE,[1] T. J. LEE,[1] J. H. COPELAND,[1] J. L. EASTMAN,[1] C. L. ZIEGLER,[2] AND C. A. FINLEY[1]

[1]*Colorado State University, Department of Atmospheric Science, Fort Collins, Colorado 80523 USA*
[2]*Mesoscale Research and Applications Division, National Severe Storms Laboratory, 1313 Halley Circle, Norman, Oklahoma 73069 USA*

Abstract. This paper utilizes United States Geological Survey (USGS) data to investigate the influence of landscape structure on atmospheric circulations. The procedure to insert this data in the Regional Atmospheric Modeling System (RAMS) is described. Simulations are presented for a monthly simulation of summer weather in the United States, for case studies of cumulonimbus convection along a dryline in the Great Plains of the U.S. and over northern Georgia, and for pollutant dispersal in South Carolina. These results demonstrate the significant role that landscape, including its spatial heterogeneity, has on weather and climate. Environmental policy-makers need to consider this feedback to weather and climate, rather than just assuming the atmosphere is an external factor to such issues as ecosystem management and water resource management. This feedback between the atmosphere and the land surface needs to be considered on all spatial scales from the plot scale to the global scale. This includes studies being performed at the Long-Term Ecological Research (LTER) sites that have been established throughout the United States. This paper also demonstrates the value of the USGS data in weather and climate simulations.

Key words: climate change; land surface processes; land use data; mesoscale atmospheric modeling; RAMS (Regional Atmospheric Modeling System); regional atmospheric modeling; U.S. Geological Survey land cover data.

INTRODUCTION

The importance of land surface processes to weather and climate is becoming more recognized (e.g., Cotton and Pielke 1995). For example, studies that document the modification of atmospheric boundary layer structure, and/or the development of mesoscale flow due to land surface inhomogeneity are reported in Pielke et al. (1991, 1993), Dalu et al. (1991), Cotton and Pielke (1995), Segal and Arritt (1992), Avissar and Pielke (1989), Manqian and Jinjun (1993), Raupach (1991), Guo and Schuepp (1994), Avissar and Chen (1993), and André et al. (1989*a*). Observations have documented the importance of heterogeneous landscape in influencing boundary layer structures and mesoscale fluxes. (Balling 1988, Segal et al. 1988, 1989, Beljaars and Holtslag 1991, Doran et al. 1992, Smith et al. 1992, Mahrt and Ek 1993, Mahrt et al. 1994*a*, *b*) and in affecting such related properties as soil water infiltration (Wood et al. 1992).

Field programs have been undertaken with a focus on land surface-atmospheric interactions. These include FIFE (First International Satellite Land Surface Climatology project-ISLSCP Field Experiment; Sellers et al. 1992, Betts and Beljaars 1993) in Kansas, USA; BOREAS (Boreal Ecosystem-Atmosphere Study; see Experiment Plan 1993) in Saskatchewan and Manitoba, Canada; LOTREX (LOngitudinal land-surface TRansverse EXperiment; Schädler et al. 1990) in Hildesheimer Börde, Germany; EFEDA (ECHIVAL Field Experiment in a Desertification-threatened Area; Bolle et al. 1993) in Spain; HAPEX-MOBILHY (Hydrological and Atmospheric Pilot EXperiment and MOdélisation du BILan HYdrique; André et al. 1989*b*, Noilhan et al. 1991) in France; HAPEX-NIGER92 (Gash et al. 1991); SEBEX (Sahelian Energy Balance EXperiment in Niger in 1992; Wallace et al. 1991) in the Sahel of Africa and in the Amazon region (e.g., Shuttleworth 1985, Gash and Shuttleworth 1991, Wright et al. 1992).

However, it has been found that adequate data to properly characterize the land surface have been missing. The U.S. Geological Survey's (USGS) effort to describe landscape has begun to remedy this deficiency.

In the following section, our use of USGS data is summarized. These data have been instrumental in completing new research studies, including the construction of procedures to parameterize landscape het-

Manuscript received 21 December 1994; revised and accepted 10 November 1995; final version received 12 March 1996. For reprints of this Invited Feature, see footnote 1, p. 1.

erogeneity using methodologies such as proposed in Zeng and Pielke (1995) and Pielke et al. (1996).

USE OF USGS DATA

RAMS geography files and surface data ingesting system

Many of the recent atmospheric models include a surface module that calculates land surface hydrology. As described in Lee et al. (1993) and Lee and Pielke (1996), the Colorado State University Regional Atmospheric Modeling System (RAMS) geography files are used to provide the RAMS surface submodel with land surface boundary conditions that are necessary to perform a model simulation, where the land surface boundary conditions generally consist of land cover, land use, and elevation. The RAMS geography data files include topography files (e.g., global data for both 10 and 5 arcminutes; U.S. data for every 30 arcseconds) and land cover files (e.g., global data for every 1 arcdegree; U.S. data for every 30 arcseconds) at different resolution. The data are saved in $1° \times 1°$ blocks and the geographic coordinate of the southwest corner of the block is used as the data file name. For instance, a data file name of ''V40N105W'' indicates that the data stored in this file represent vegetation cover over a geographic region of 40°–41° north and 104°–105° west. The data files are encoded using a ''v-format'' in which each data point is saved in two printable ASCII characters. In order to access the data, a RAMS data decoder must be used and a RAMS model grid must be determined in advance.

The RAMS uses a telescoping nested grid mesh. The grid mesh is in an oblique spherical polar stereographic projection and is determined by (a) coordinates of the center of the projection, (b) coordinates of the center of the grids, (c) number of grid points in x and y directions, and (d) grid increments in the two directions. Plate 1a shows a three-tier grid structure with a 100-km grid increment 40 by 32 coarse mesh, a 20-km grid increment 37 by 42 middle mesh, and a 4-km grid increment 52 by 42 fine mesh. The grids are centered at (39.75° N, 105° W), (39.75° N, 103° W), and (39.22° N, 104.2° W), respectively, and with the map projection centered at (30° N, 100° W). Once the model grids have been determined, the RAMS data-ingesting module can access the data files and perform necessary operations. Due to data sampling and numerical constraints, topographic data must be filtered. This technique was reported in Lee and Pielke (1996).

After having the topography data ingested into the model, the next task is to obtain land use and land cover data for insertion into the model. Unlike the topography data, in which a numerical filter can be applied to remove undesired, small-scale features, the classification of land use and land cover categories cannot be straightforwardly averaged or filtered in the form in which this information is normally available. Although we can average the fundamental parameters that were used to develop the classifications, the current application of land use data in RAMS has been to utilize the most frequent classification that is observed in a grid box.

The USGS land cover data (Loveland et al. 1991, Brown et al. 1993) were first converted to a BATS (Biosphere-Atmosphere Transfer Scheme) classification (Dickinson et al. 1986, 1993) and then the dominant class for all the pixels in a grid box was chosen to represent the grid box. The percentage of water coverage (not shown) in a grid box, which is also a land cover parameter used by RAMS, can also be obtained simply by counting the pixels that are classified as water. Finally, the leaf area index (LAI) used by RAMS can be obtained from the USGS Normalized Difference Vegetation Index (NDVI) data (Eidenshink 1992) using a similar technique. Plate 1b–d shows an example of the USGS land cover data mapped onto the three model grids.

Incorporation of land use data in monthly simulations of U.S. weather

We have begun to examine the effects of surface characteristics, in particular vegetation, on the regional climate across the United States. We are using the RAMS (Pielke et al. 1992) to perform sensitivity simulations to both the specification of and changes in vegetation distribution. The sensitivity to specification of the vegetation distribution may arise from different methods of aggregating the raw data into broad vegetation type categories. Changes in vegetation distribution from the current natural state can result from natural (climate change) or anthropogenic (agricultural practices, climate change) causes.

Prior to attempting climate sensitivity scenarios we need to verify that the model is capable of recreating the current climate. The RAMS climate verification simulations for July 1992 (not shown) and July 1993 (shown) use National Meteorological Center (NMC) analyses as initial and boundary conditions filtered to 2000-km resolution. Model-generated climatology is verified by reference to analyses of station observations for the same period. The model domain has a constant horizontal grid separation of 60 km on a stereographic grid covering the conterminous United States. The format of the RAMS model used for each simulation in our paper is summarized in Table 1. There are 20 vertical levels from 119 m AGL up to 22 895 m AGL. Plate 2 shows the topography resolved on a 60-km mesh. The vegetation distribution used in these simulations is derived from the USGS Conterminous U.S. Land Cover Characteristics Data Set (Loveland et al. 1991) recategorized to the 18 BATS classes. Plate 3 shows the vegetation on the RAMS grid.

July 1993 climate verification.—For this case, initial and boundary conditions were obtained from filtered

NMC 12-h analyses. RAMS was run from 0000 GMT (Greenwich Mean Time) 1 July 1993 through 0000 GMT 1 August 1993. Comparisons are made between analyses of average daily surface temperature and total precipitation from the Climate Analysis Center (1993) and the RAMS simulation.

1. *Climatology*.—July 1993 will be most remembered for the extreme flooding in the lower Missouri and Upper Mississippi River Valleys. Nationwide July 1993 was a particularly cold month, but what is most surprising is that it was also the eighth driest July of the past century. The regional temperature pattern can be simply summed up as cold in the Northwest and hot in the Southeast. The Pacific Northwest had the coldest July on record and both the remaining Pacific Coast and Northern Rocky Mountain and Plains regions had the second coldest July on record. In contrast, just about every state east and south of the Mississippi and Ohio rivers had the hottest July on record. Fig. 1 shows the average temperature pattern for the month. Average temperatures exceeded 30°C for large areas of Texas, Georgia, and South Carolina. Average temperature anomalies were from 2°C to 3°C above normal in these regions. In the Northern Plains region of the Dakotas, Montana, and Wyoming, where average temperatures were below 20°C, the anomalies approached 6°C below normal.

The wet regions for July 1993 were confined to the Missouri and upper Mississippi river basins and the northernmost states west of this region (Fig. 2). Each of those states recorded one of their three wettest Julys on record. In contrast most of the remaining states had one of their ten driest Julys, particularly in the Southeast and Southwest. In terms of actual precipitation totals (Fig. 2) the maximum areas were in the eastern Kansas–Iowa region and around the Mississippi delta. Both areas had in excess of 200 mm of rainfall with maxima from 300 to 400 mm. Outside of the west the major dry region extended from central Texas through Arkansas and Tennessee and along the Appalachians.

2. *Model results*.—The model surface temperatures were obtained using the Louis (1979) similarity theory formulation over bare soil and vegetated surfaces. The screen height (1.8 m) temperatures over bare soil and vegetation were averaged using the vegetation fraction as a weight. Plate 4 shows the resulting average screen height temperature pattern. The model has again done a good job in reproducing the correct temperature pattern. Overall the average temperatures are in very good agreement with observations. There does exist a slight cool bias in Texas and the scrublands of the western intermountain regions. This may be due to an overestimation of the vegetation fraction by the BATS classes. One of the drawbacks of the BATS vegetation classes is the lack of regional diversity in the vegetation parameters. For example, the fractional coverage of coniferous forests and their leaf area index, in the BATS categorization, is the same in Washington, Colorado, and Georgia. The vegetation fraction used in weighting the bare soil and vegetation screen height temperatures is almost uniformly 80%, except for desert (0%), semidesert (10%), and tundra (60%) classes. In all areas the screen height temperature over vegetation was cooler than the observed temperature. Use of a vegetation fraction that is too high would result in an underestimation of the screen height temperature.

The model has done a good job at reproducing the pattern of precipitation while falling short of the actual amount (Plate 5). The model has picked up both the wet regions in eastern Kansas and along the Gulf Coast, along with the dry region from Texas up the Appalachians. A problem with the simulation of quantitative precipitation amounts is related to the soil moisture initialization. Beljaars et al. (1996) demonstrated that a requirement for realistic simulation of precipitation is a realistic soil moisture initialization. The soil moisture initialization used in the RAMS simulation is based on the initial near-surface humidity. This poor initial soil moisture is responsible for a large portion of the order of magnitude error in precipitation amount. A later simulation of July 1989 (not shown) using a two-layer antecedent precipitation index soil moisture initialization (Chang and Wetzel 1991) led to a reduction in precipitation errors to within a factor of two of observed (Copeland 1995). The excessive precipitation in the Carolinas is the result of the use of climatological sea surface temperatures (SST). A positive SST anomaly off the southeast coast of the United States was observed for the simulation time period. The use of observed SSTs during another period of positive Atlantic SST anomaly (July 1989) led to reduced precipitation bias along the southeast coastal region (Copeland 1995).

RAMS has demonstrated its capability for regional climate simulations. The next step is to continue the sensitivity simulations with vegetation distributions corresponding with the natural state and potential distributions derived from altered climate scenarios. Another important aspect is that currently the vegetation component of the RAMS only reacts to the instantaneous values of heat and moisture. It has no memory for drought and/or flood periods. An additional sensitivity would be to force the vegetation through its growing cycle with LAI derived from the NDVI information in the USGS data set.

Effect of land use variability on precipitation patterns

This study focuses on the effects of land use patterns on moderate to deep convection, and the resulting precipitation patterns. A great deal of work has been done on surface heterogeneities and their effects on dispersion (see Pielke and Uliasz 1993), while recent work is suggesting a profound impact on precipitation events. To aid in this study, RAMS used a fine reso-

TABLE 1. Model specifications used in the experiment described in the paper. GMT = Greenwich Mean Time.

Experiment	Horizontal domain size (grid points)	Horizontal domain size (km)	Horizontal grid spacing (km)	Domain depth (km)	Vertical grid spacing† (m)
See section *Incorporation of land use data*	85 × 55	5100 × 3300	60	22.85	250–2000
See section *Effect of land use variability*	Grid 1: 70 × 70 Grid 2: 70 × 70	Grid 1: 630 × 630 Grid 2: 210 × 210	Grid 1: 9 Grid 2: 3	18.6	100–1000
See section *Influence of land surface processes*	Grid 1: 45 × 45 Grid 2: 53 × 62 Grid 3: 42 × 82 Grid 4: 73 × 98	Grid 1: 2640 × 2640 Grid 2: 1040 × 1220 Grid 3: 205 × 405 Grid 4: 72 × 97	Grid 1: 60 Grid 2: 20 Grid 3: 5 Grid 4: 1	20	100–1000
See section *Use of USGS vegetation data*	Grid 1: 28 × 28 Grid 2: 46 × 38 Grid 3: 58 × 58	Grid 1: 896 × 896 Grid 2: 368 × 304 Grid 3: 116 × 116	Grid 1: 32 Grid 2: 8 Grid 3: 2	18.65	80–1000

† Vertical grid is stretched with the smaller grid spacing near the surface. The larger grid increment is the spacing in the upper levels of the model.

lution mesh of 3 km to explicitly resolve microphysics. The model employs a parameterization of radiation that accounts for water substance (Chen and Cotton 1987), subgrid-scale turbulence, and a soil model (Tremback and Kessler 1985). On days that the synoptic forcing is weak, the mesoscale circulations tend to dominate. These circulations are mainly forced by orographic, vegetative, and soil moisture/class variability. The RAMS model takes all of these variations into account. Land use is investigated through the use of a vegetation algorithm based originally on McCumber (1980). The vegetation is classified by first ingesting the USGS vegetation data, of which there are 159 classes. These classes are then further grouped into 18 classes, as defined by the BATS classification scheme. The vegetation distribution for the fine grid is shown in Plate 6.

A case day was selected that is typical of a stagnant high-pressure system centered over the southeastern United States. Low-level winds were quite weak and provided a good setting to study the impacts of the vegetative variability prevalent in the Atlanta, Georgia area. On 26 July 1987 a substantial amount of cumulus convection was visible from satellite imagery throughout the morning hours. At ≈1300 EST (Eastern Standard Time) the convection became more organized and a rather substantial system of cumulus convective cells developed over the Atlanta area. This system persisted a few hours before it began to decay.

There were two RAMS simulations performed for this study. In both cases the model was homogeneously initialized with a sounding taken from Athens, Georgia, and the topography was initialized using 30-arc second topographical data. In the control simulation the vegetation was initialized to its current spatial patterns according to USGS data. For these runs, except for the forested regions, the other land use patterns were assumed to be water stressed, such that transpiration was minimal. In the other simulation the vegetation was set to a constant value that represented mixed woodlands. This would crudely represent the land use characteristics before settlement occurred. All other characteristics were kept the same for both simulations.

The simulations were integrated 12 h forward in time starting at 0700 LST (Local Standard Time) and the developing fields were compared. Plate 8 shows isosurfaces of the total condensate mixing, set to a value of 10^{-4} kg/kg. The view is elevated, looking from the south, with Atlanta in the center of the domain. The colored *x-y* plane is the USGS-derived vegetation distribution employed by each simulation. Notice that by 1400 LST, the large cell that has developed in the variable vegetation simulation, while the constant vegetation case shows little convective activity at this time. A large spatial area has received precipitation in the variable land use case, while the homogeneous simulation shows little accumulated precipitation. It is not until late afternoon that the homogeneous case begins to accumulate any significant precipitation amounts. There is also a clear contrast in the spatial patterns of the rain, with the homogeneous case appearing to rain in areas where orographic forcing of the north Georgia mountains provides the main forcing of the mesoscale circulation. The impact of the variable vegetation is readily seen and is due to the organization of mesoscale circulations, especially when weak synoptic forcing is present.

Influence of land surface processes on development of deep convection on the dryline in the Great Plains

The dryline of the U.S. High Plains is a boundary separating warm, moist air extending northward from the Gulf of Mexico from hotter, drier air originating in the intermountain region of Mexico and the southwest U.S. (e.g., Schaefer 1973, Ziegler and Hane 1993). The dryline is a favored location for thunderstorm formation during the spring and early summer months (Rhea 1966). Mixing of warm, dry air aloft with cooler, moist boundary layer air just above the surface causes the

TABLE 1. Continued.

Initial conditions	Lateral boundary conditions	Topography	Vegetation soil
0000 GMT 1 July 1993, synoptic analysis	updated every 12 h from synoptic analysis	30″ USGS	30″ USGS
1200 GMT 26 July 1987, horizontally homogeneous vertical profile moistened below 70 mPa	open, updated based on interior values	30″ USGS	30″ USGS or homogeneous
1200 GMT 15 May 1991 synoptic analysis	updated every 12 h from synoptic analysis	Grid 1: 10′ USGS Grid 2: 10′ USGS Grid 3: 30″ USGS Grid 4: 30″ USGS	30″ USGS and specified short grass/sandy clay loam
1200 GMT 24 May 1990 synoptic analysis	updated every 12 h from synoptic analysis	30″ USGS	30″ USGS clay loam

dryline to move eastward during the daytime (e.g., Schaefer 1973). In the present discussion, we collectively refer to the region experiencing boundary layer mixing and convective initiation, up to 100 km east of the dryline and 1000 km along the dryline in the north–south directions, as the ''dryline environment.''

We have performed coupled simulations of the dryline environment, the dryline itself, and deep moist convection along the dryline using RAMS. We simulate the dryline of 15 May 1991, one of four drylines extensively observed during the COPS-91 field experiment conducted in the Texas–Oklahoma–Kansas region during the spring of 1991 (Hane et al. 1993). Several mesoscale modeling studies over the last decade have simulated aspects of the dryline environment in two and three dimensions with increasing spatial resolution and detail of the physical parameterizations of the land surface and soil layer. In this paper, we report preliminary results of simulations of the dryline and its environment using the three-dimensional version of RAMS. The 15 May case is of special interest because tornadic dryline convection developed in the same environment as observed by the NOAA (National Oceanic and Atmospheric Administration) P-3 aircraft and the National Severe Storms Laboratory (NSSL) mobile class sounding system, and because the dryline environment was observed for ≈10 daylight hours.

We employ four grids (Plate 7) with terrain interpolated to the outer two grids from a 10-arcminute resolution (lat-lon) data set and from a 30-arcsecond terrain data set on the inner two grids. The outermost 45×45 (x,y) grid has a 60-km horizontal grid spacing (i.e., 2640×2640 km) and Δt (where Δt denotes the time interval between successive model calculations) $= 80$ s; the first nested grid (53×83) has a 20-km grid spacing (i.e., 1040×1640 km) and $\Delta t = 40$ s; and the second nested grid (54×82) has a 5-km horizontal grid spacing (i.e., 265×405 km) and $\Delta t = 20$ s. The finest grid (72×97) has a 1-km horizontal grid spacing with $\Delta t = 5$ s. The finest grid is designed to explicitly resolve deep, moist convection, while the 5-km grid should coarsely resolve the dryline itself. The outer 20-km and 60-km grids characterize the dryline environment. Atmospheric grids are terrain-following and vertically stretched from $\Delta z = 100$ m at the surface (lowest level = 49 m) to $\Delta z = 1000$ m at and above 13 km, and the total depth is ≈20 km, where Δz is the vertical grid interval used in the model. The soil model is separated into 11 layers spaced 3 cm apart.

Initial atmospheric fields have been generated by blending NMC pressure analyses with standard radiosonde soundings and a surface observation analysis on a grid whose vertical coordinate surface is at constant potential temperature and entropy (i.e., isentropic). This coordinate surface is used because interpolation of temperature data to grid points is more accurate on isentropic surfaces than on constant height surfaces, thus better preserving the true character of thermal discontinuities. To resolve the moist layer east of the dryline, we employed 1°K (degree Kelvin) contour intervals from the surface through the boundary layer. Successively coarser temperature contour values of 2, 5, and 10 K are used with increasing elevation above the boundary layer. Our data analyses reveal that the synoptic environment of the 15 May dryline is dominated by the confluence of a southerly current carrying gulf moisture with dry westerly winds from northern Mexico and the intermountain region of the southwest United States (not shown). This zone of confluence is positioned over western Texas and eastern Colorado at sunrise. As will be illustrated by our simulation results, the zone of confluence shifts eastward during the day and coincides with sharpening of the west–east moisture gradient as the dryline forms.

Two key land characteristics for our dryline simulations are soil moisture and vegetation type (land use). Soil moisture has been initialized using a technique based on the Antecedent Precipitation Index or API (Wetzel and Chang 1988). The API technique is based on series of 24-h total precipitation values, which are

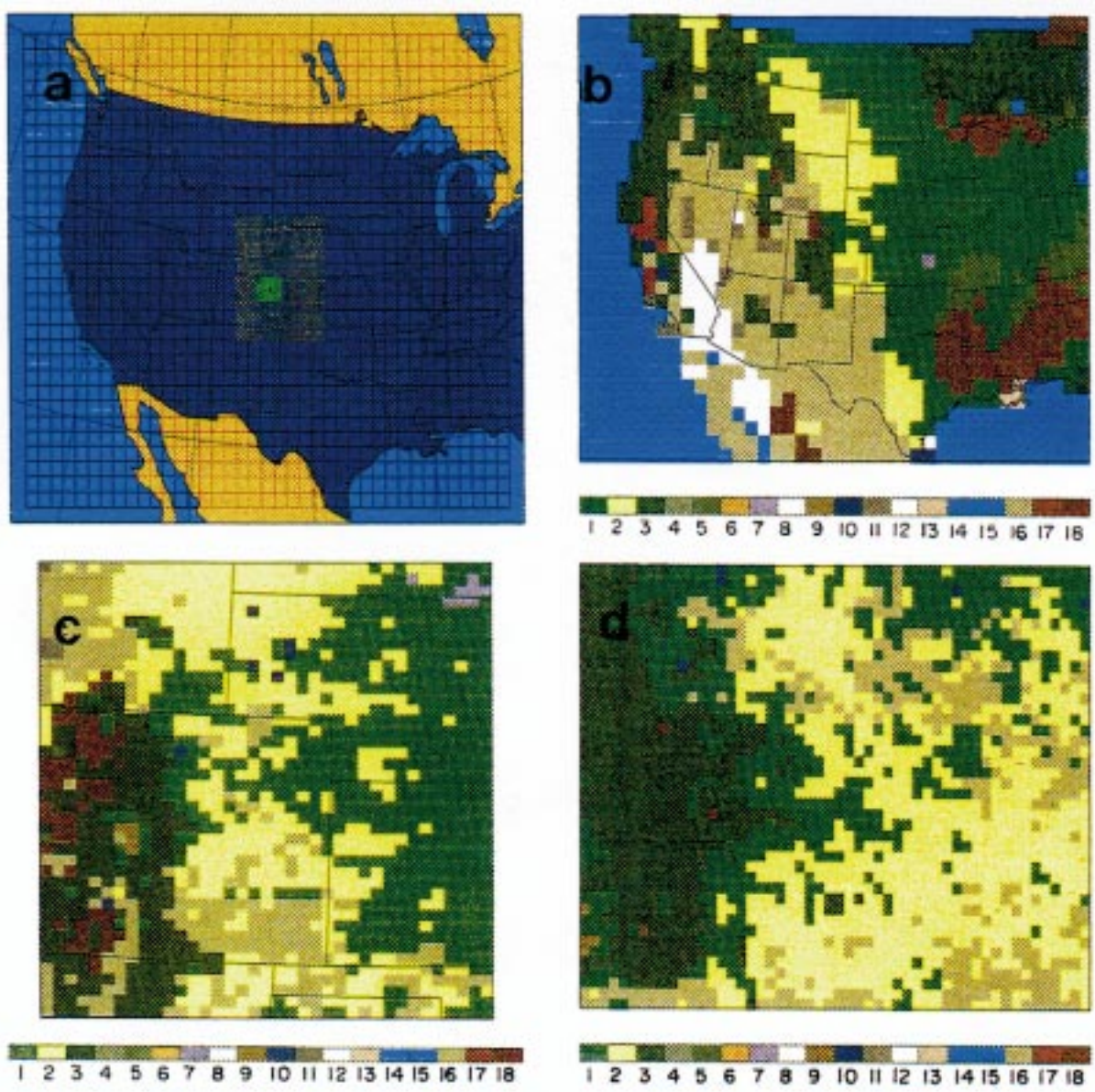

PLATE 1. A three-tier RAMS (Regional Atmospheric Modeling System) grid structure (a) and the USGS land cover data mapped onto each of the three grids (b-d).

derived from hourly precipitation data (HPD). The 24-h total precipitation data are synthesized over a 6-mo period employing a first-order autoregressive model that parameterizes bulk evapotranspiration from the surface. The bulk soil moisture percentage S is computed from API at the location of each HPD site, and S values are then horizontally interpolated to the model grids. To approximate the effect of antecedent drying of upper soil layers, we have adjusted the surface and rooting-zone soil layer moisture values downward to a

→

PLATES 2–3. Plate 2 (top): Resolved topography on the 60 km RAMS grid, from a 10-arc minute digital elevation model. Contours from 100 to 3100 m by 200 m. Plate 3 (bottom): BATS (Biosphere-Atmosphere Transfer Scheme) vegetation classes derived from the USGS Land Cover Data Set. (1 crop/mixed farming, 2 short grass, 3 evergreen needleleaf tree, 4 deciduous needleleaf tree, 5 deciduous broadleaf tree, 6 evergreen broadleaf tree, 7 tall grass, 8 desert, 9 tundra, 10 irrigated crop, 11 semidesert, 12 ice cap/glacier, 13 bog or marsh, 14 inland water, 15 ocean, 16 evergreen shrub, 17 deciduous shrub, 18 mixed woodland.)

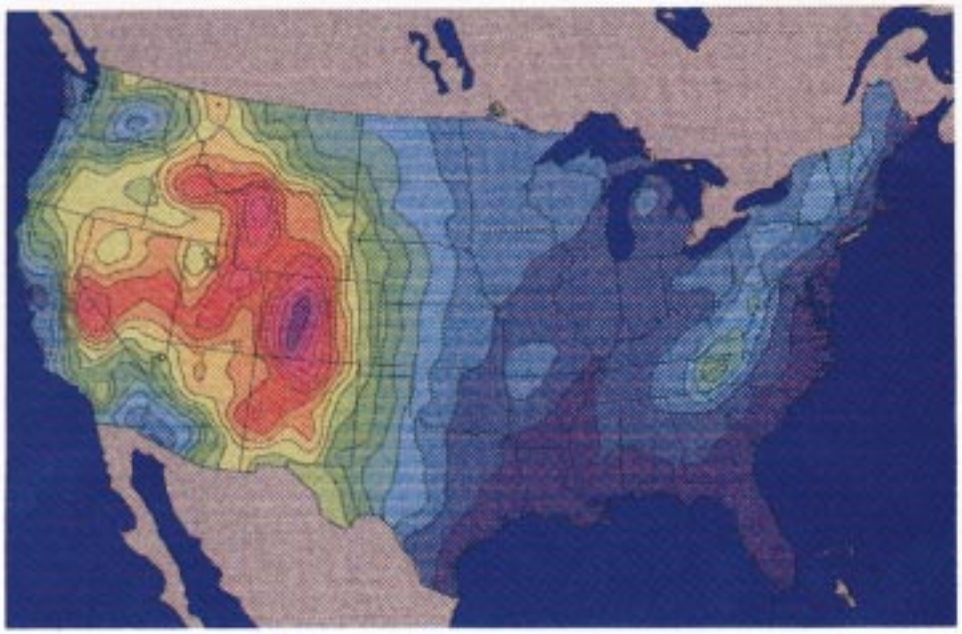

100 300 500 700 900 1100 1300 1500 1700 1900 2100 2300 2500 2700 2900 3100

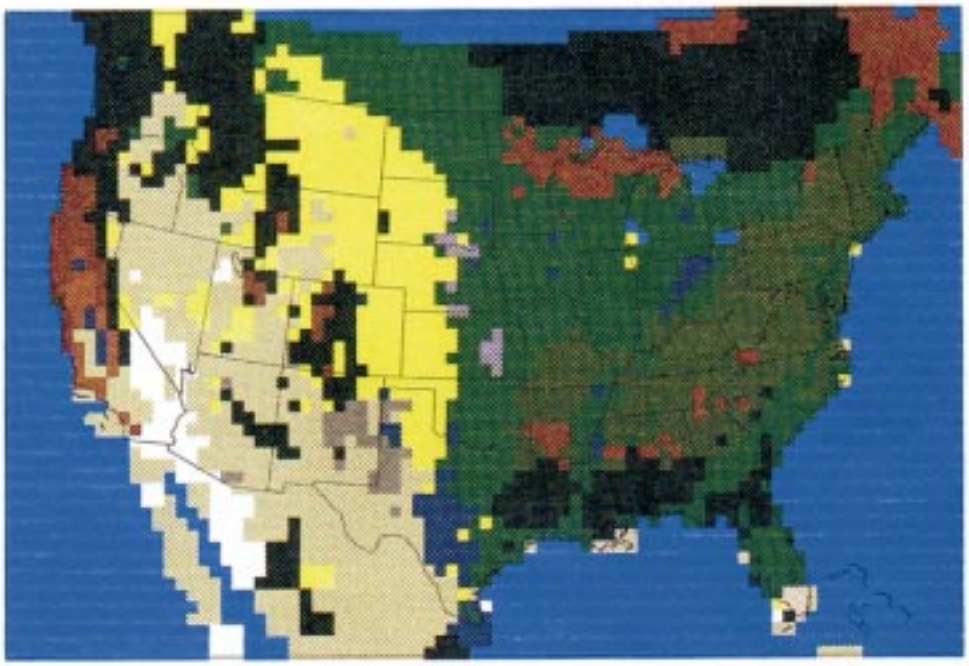

1 2 3 4 5 6 7 8 9 10 11 12 13 14 15 16 17 18

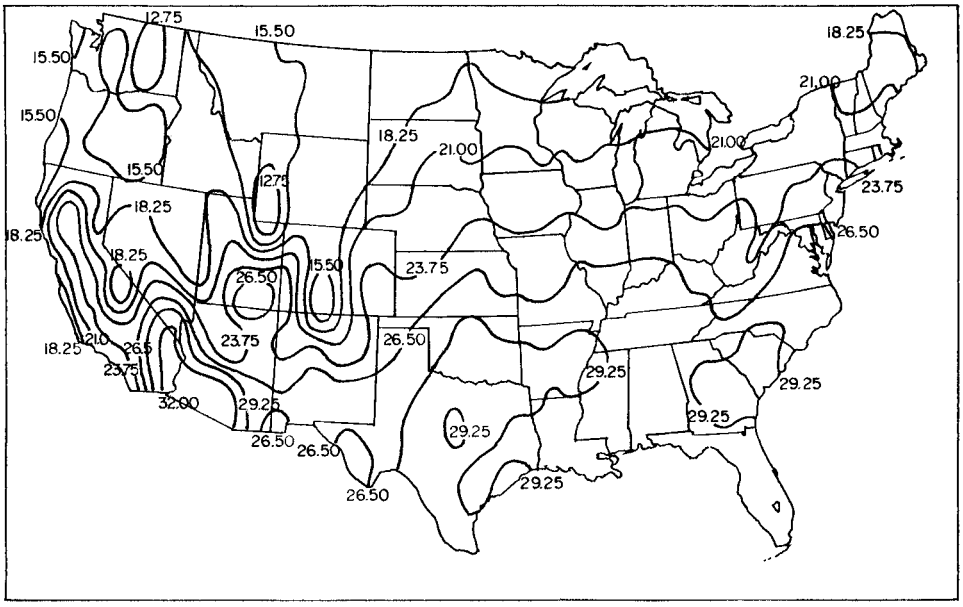

FIG. 1. July 1993 average temperature (°C) (Climate Analysis Center 1993). Contours indicate changes of 2.75°C.

percentage of the interpolated *S* value, a method similar to that used by Lee (1992). The analyzed soil moisture on 15 May (not shown) is highly variable and increases from west to east over the dryline-prone region of the southern plains, stimulating strong differential heating that forces dryline formation (Ziegler et al. 1994). The soil temperature profile is based on the analyzed surface temperature. In these preliminary runs we assume sandy clay loam soil. In two sensitivity test runs reported in this paper, we assume: (a) short grass vege-

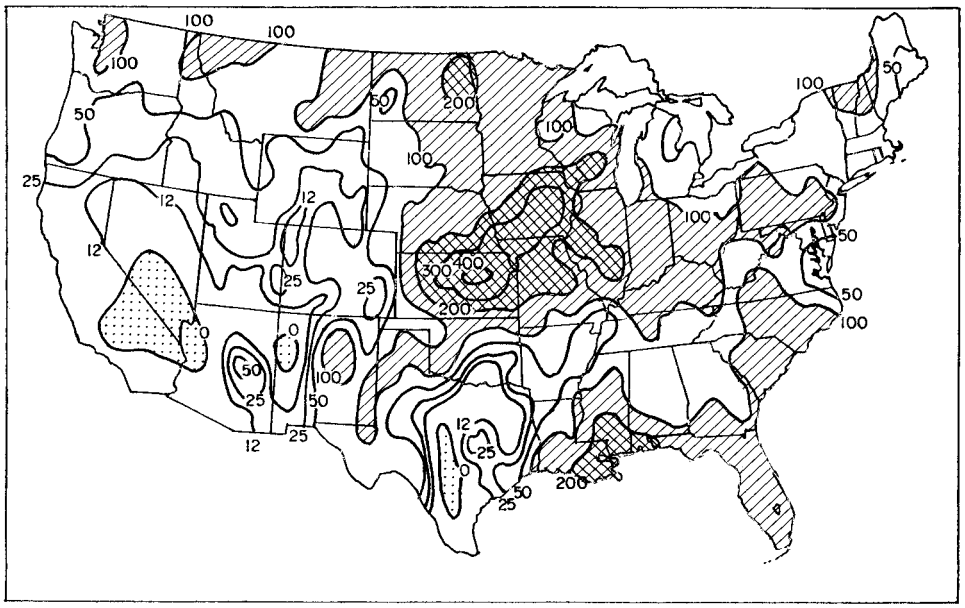

FIG. 2. July 1993 total precipitation (Climate Analysis Center 1993). Contours are at 12, 25, 50, 100, 200, 300, and 400 mm. Dotted areas represent a value of zero precipitation; hatched areas represent values between 100 and 200 mm, and cross-hatched areas represent values >200 mm.

→

Plates 4–5. Plate 4: RAMS July 1993 average temperature (°C). Plate 5: RAMS July 1993 total precipitation (mm). The maxima in the Missouri Valley are near 40 mm. Contours from 5 mm to 75 mm by 10 mm.

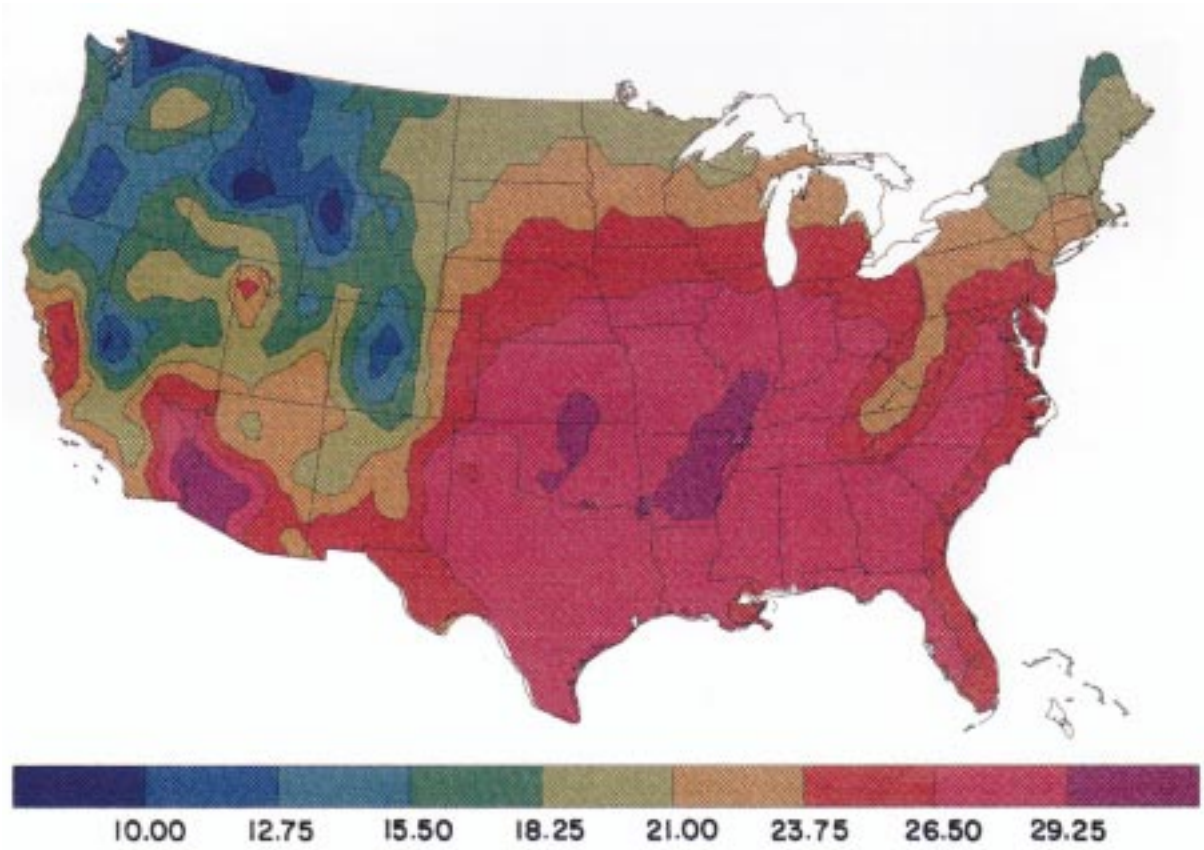
10.00
12.75
15.50
18.25
21.00
23.75
26.50
29.25

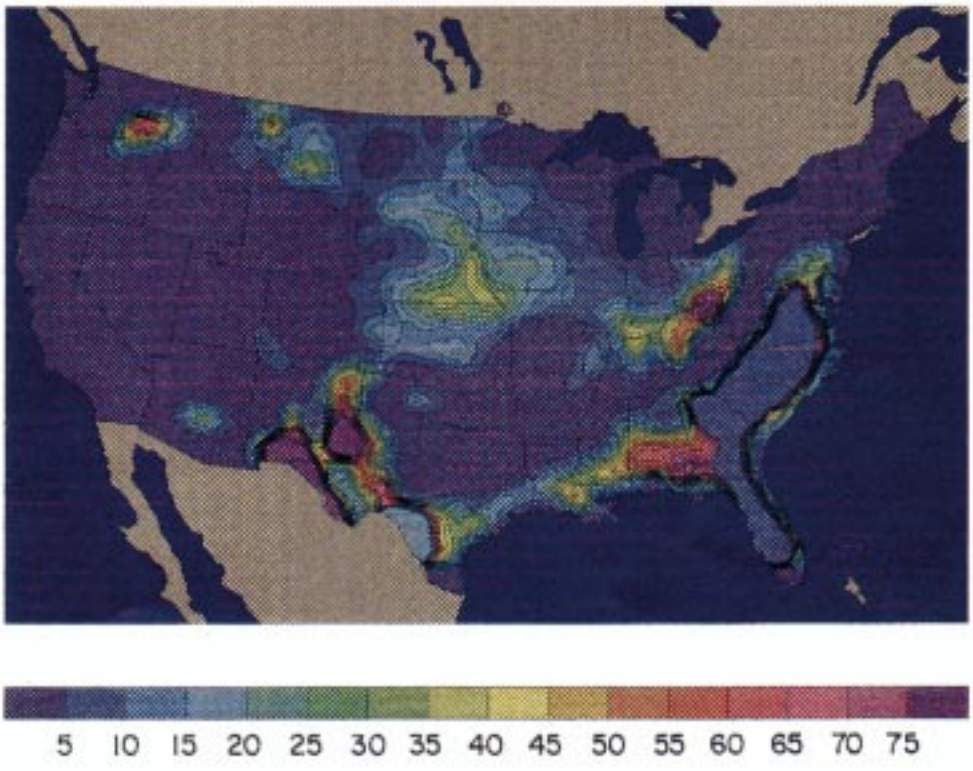
5
10
15
20
25
30
35
40
45
50
55
60
65
70
75

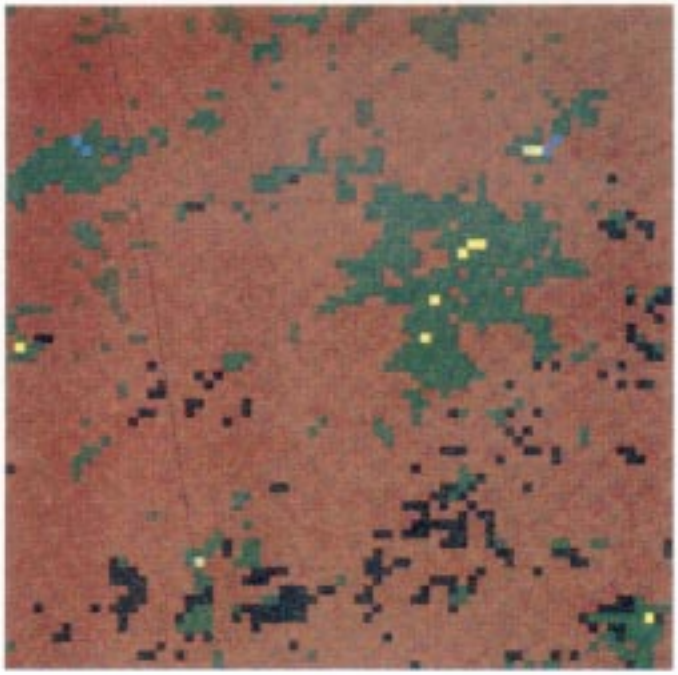

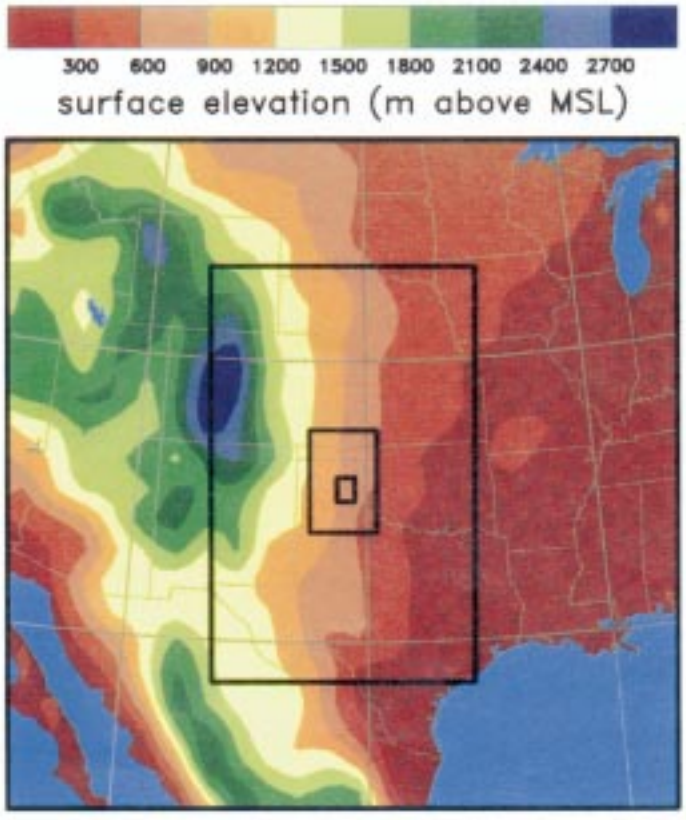

PLATES 6–7. Plate 6 (top): Viewed from above, the modeling domain and vegetation distribution for north Georgia. For vegetation class codes see Plate 3. Plate 7 (bottom): Model terrain (m above mean sea level [MSL]) and grid configuration for the 15 May 1991 dryline simulations. The outer dimensions of the figure denote the outermost grid, while nested grids of increasing resolution are also indicated.

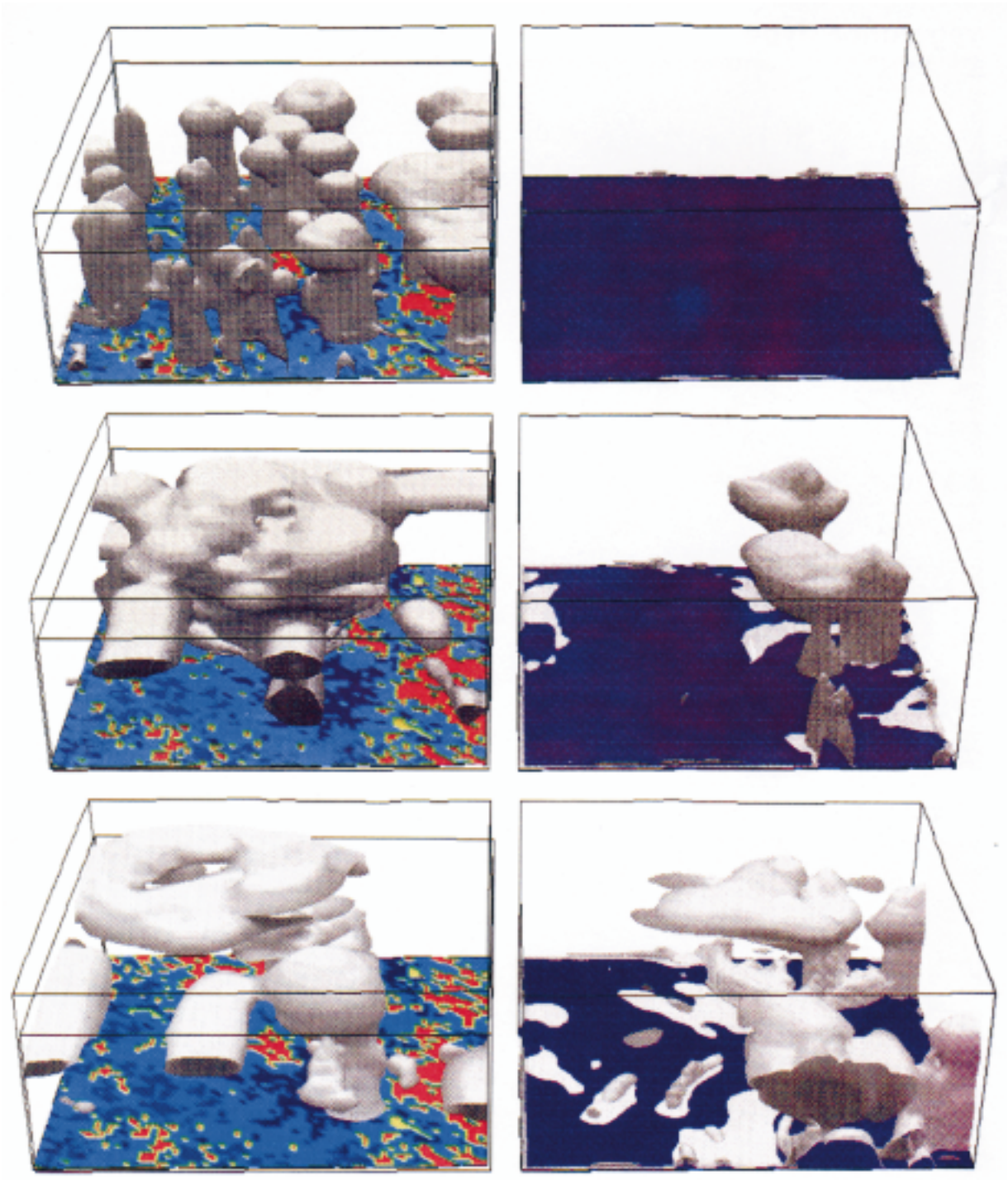

PLATE 8. (Top) Perspective view of the Atlanta area, looking from the south of the landscape and the clouds. Gray surfaces represent isosurfaces of condensate mixing ratio, set to 1×10^{-4} kg/kg. The plane represents vegetative variation. Current vegetation simulation is on the left, homogeneous simulation on the right. Time is 1100 LST (Local Standard Time). (Middle) Same as top but taken at 1400 LST. (Bottom) Same as top, but taken at 1600 LST.

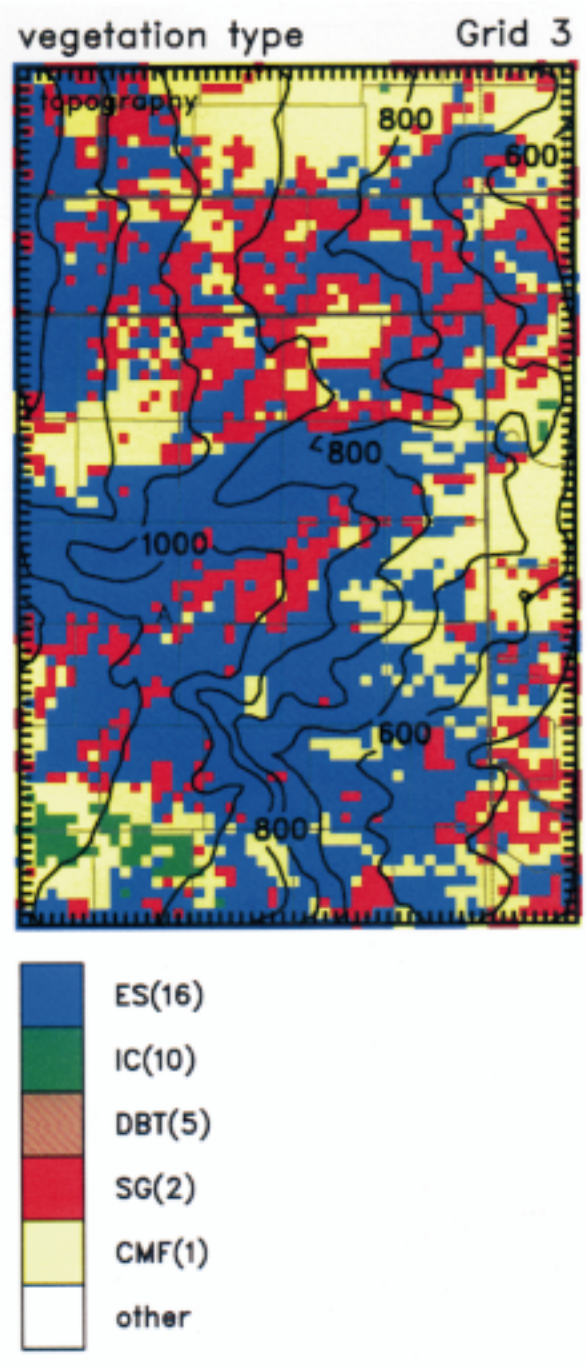

PLATE 9. USGS land cover data (color-filled pixels) and topography (contours) on the second nested grid used in the 15 May 1991 dryline simulation (5-km grid increment). The predominant USGS land cover class has been converted to a BATS classification (Dickinson et al. 1986). From top to bottom the color bar depicts the following BATS categories (numerical value of BATS category in parentheses): evergreen shrub (ES), irrigated crop (IC), deciduous broadleaf tree (DBT), short grass (SG), crop/mixed farming (CMF), and other miscellaneous land cover types (other).

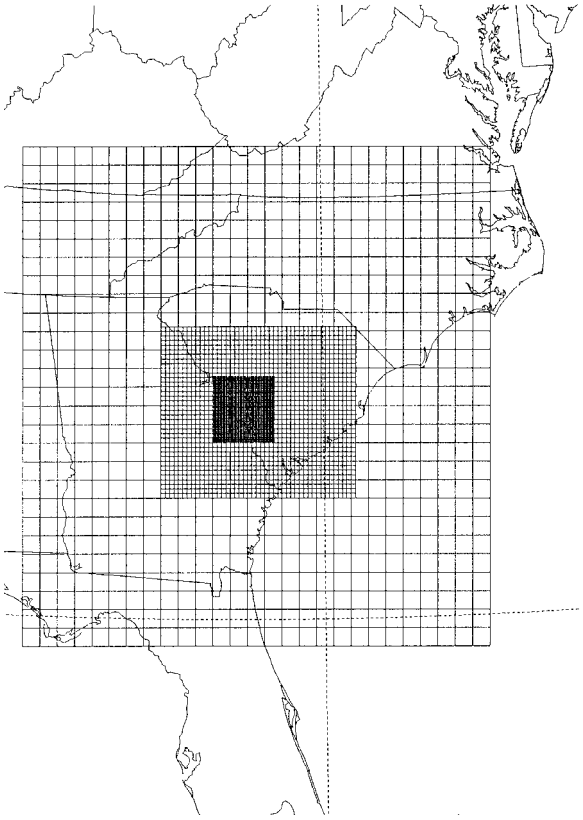

FIG. 3. Grid setup used in the SRL (Savannah River Laboratory) simulations. Grid dimensions are as follows: Grid 1: 28 × 28 points, $\Delta x = \Delta y = 32$ km; Grid 2: 46 × 38 points, $\Delta x = \Delta y = 8$ km; Grid 3: 58 × 58 points, $\Delta x = \Delta y = 2$ km.

tation everywhere; (b) variable vegetation type based on the USGS land cover data. The input USGS vegetation analysis for grid 3 is depicted in Plate 9, while examples of the vegetation analysis at other grid resolutions are presented elsewhere in the paper.

The model has been integrated from 1200 GMT (Greenwich Mean Time) 15 May to 0000 GMT 16 May 1991 using the two vegetation specifications. Although the 60-km and 20-km grids are of sufficient horizontal resolution to resolve gross features of the dryline environment, our simulations demonstrate that the 5-km grid is required to begin to resolve the thermal and airflow gradients marking the dryline itself (e.g., Hane et al. 1993, Ziegler and Hane 1993, Ziegler et al. 1994). Inspection of results on the 5-km grid (Plate 10) indicates that the peak horizontal moisture gradient is colocated with a zone of strong horizontal convergence, reinforcing the notion that the resulting east–west moisture flux convergence is responsible for the sharpening of moisture gradients at the dryline (Ziegler et al. 1994). The results on the 5-km grid also reveal multiple moisture gradients, similar to ''multiple drylines'' reported by Hane et al. (1993), whose location downstream from a moist, high LAI region in south-

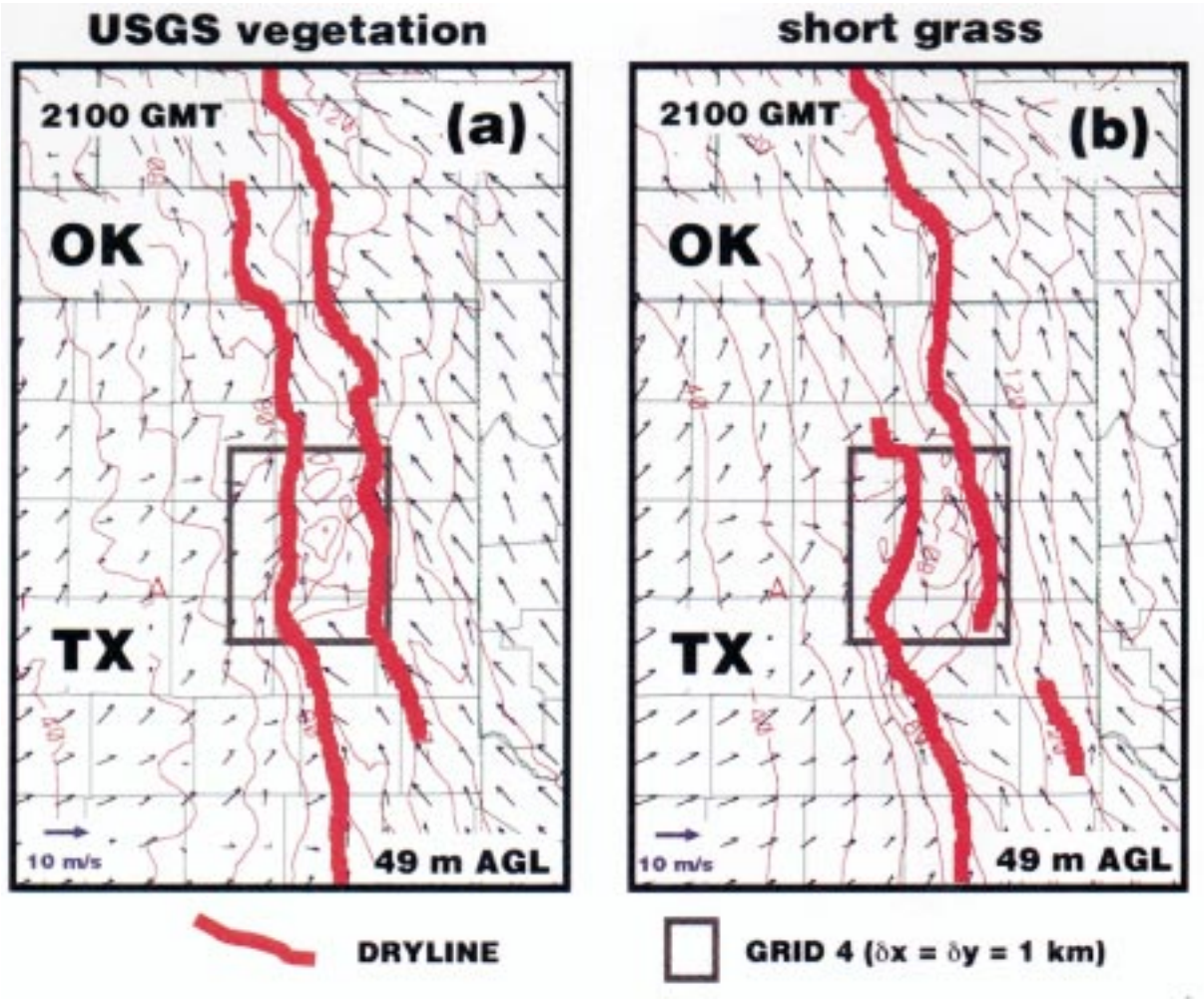

PLATE 10. Water vapor mixing ratio (g/kg) and vector horizontal velocity at z = 49 m AGL (above ground level) on the second nested grid at 21 GMT (Greenwich Mean Time) on 15 May 1991. Results are contrasted for the cases of USGS vegetation (a) and short grass (b). The vapor mixing ratio contours (g/kg × 10) are spaced at an interval of 1 g/kg and have a low value of 4 g/kg. The locations of multiple drylines are depicted by the thick red curves, while the gray box locates the third nested grid.

west Oklahoma suggests a critical role of horizontal moisture transport near the surface. A comparison of the model output with an analysis of surface observations and P-3 aircraft data (not shown) reveals very similar fields of intense low-level moisture convergence at the dryline, believed to be crucial for initiating deep convection.

By spawning a fine (1-km) grid at the modeled dryline from the parent 5-km grid (e.g., Plate 7), restarting the model at 1900 prior to cloud formation, and integrating for 3 h, we have explicitly resolved the forcing for and development of deep dryline convection. The timing of deep convective initiation and the mode of convective organization (e.g., isolated cumulonimbus vs. building cumulus) are sensitive to the assumed vegetation coverage (Plate 11a vs. 11b, respectively) due to the modulation of surface layer heat flux and the resulting changes of differential heating, horizontal transport and convergence, boundary layer growth, and dryline intensification. Convection is more widespread and vigorous in the USGS vegetation case than in the short grass case by 2100 in particular, but also over the full simulation (not shown). Comparison with special mesoscale observations suggests that the model produces deep moist convection with very similar morphology to the actual convection. Hence, our preliminary findings include the following: (1) mesoscale variations of soil moisture combine with horizontal differences of vegetation type to produce strong differential heating; (2) differential heating-induced, secondary circulations and local evapotranspiration assist in developing horizontal

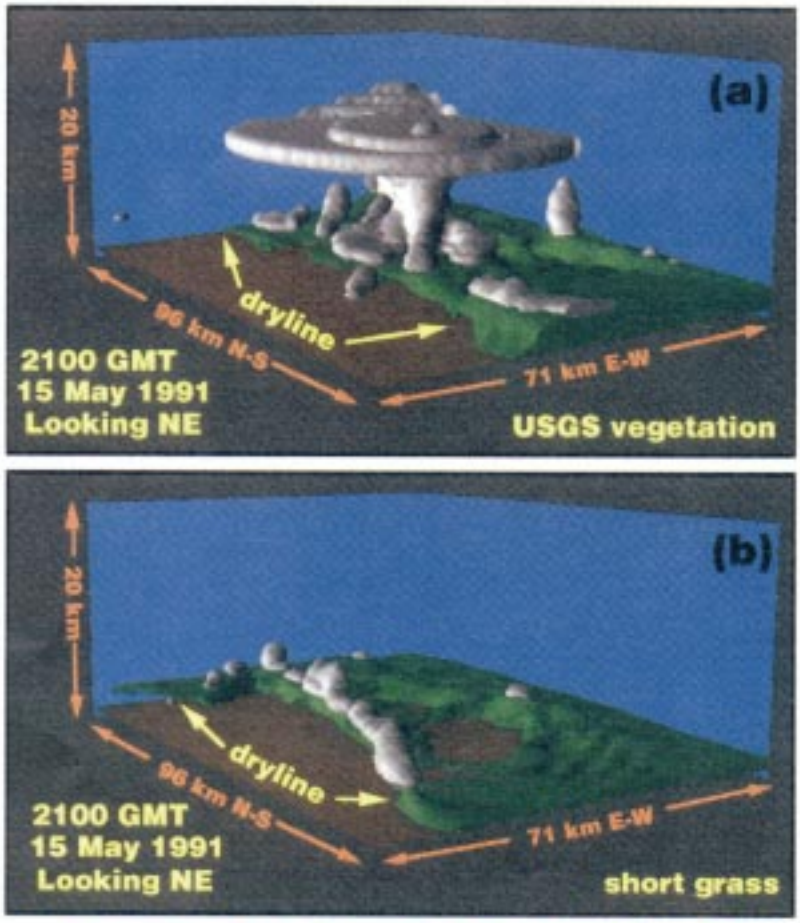
(a)
20 km
dryline
96 km N-S
71 km E-W
2100 GMT
15 May 1991
Looking NE
USGS vegetation
(b)
20 km
dryline
96 km N-S
71 km E-W
2100 GMT
15 May 1991
Looking NE
short grass

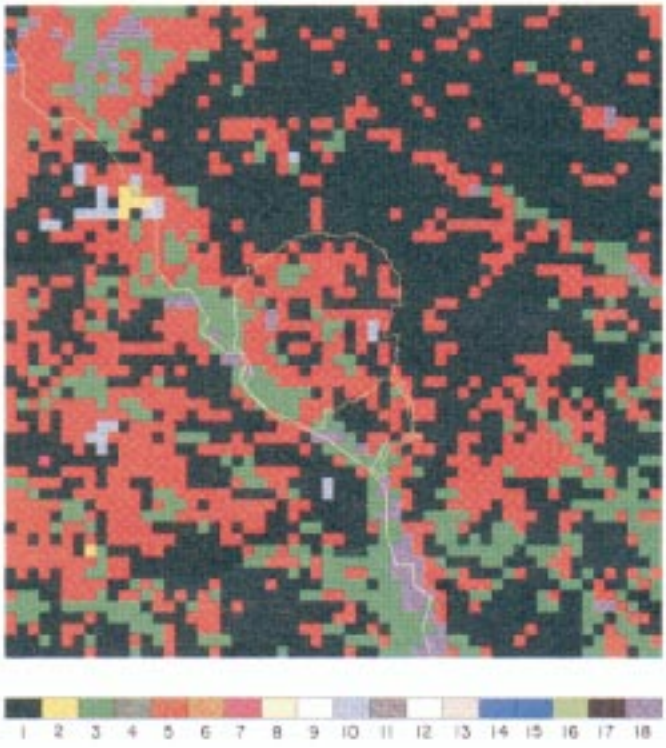
1 2 3 4 5 6 7 8 9 10 11 12 13 14 15 16 17 18

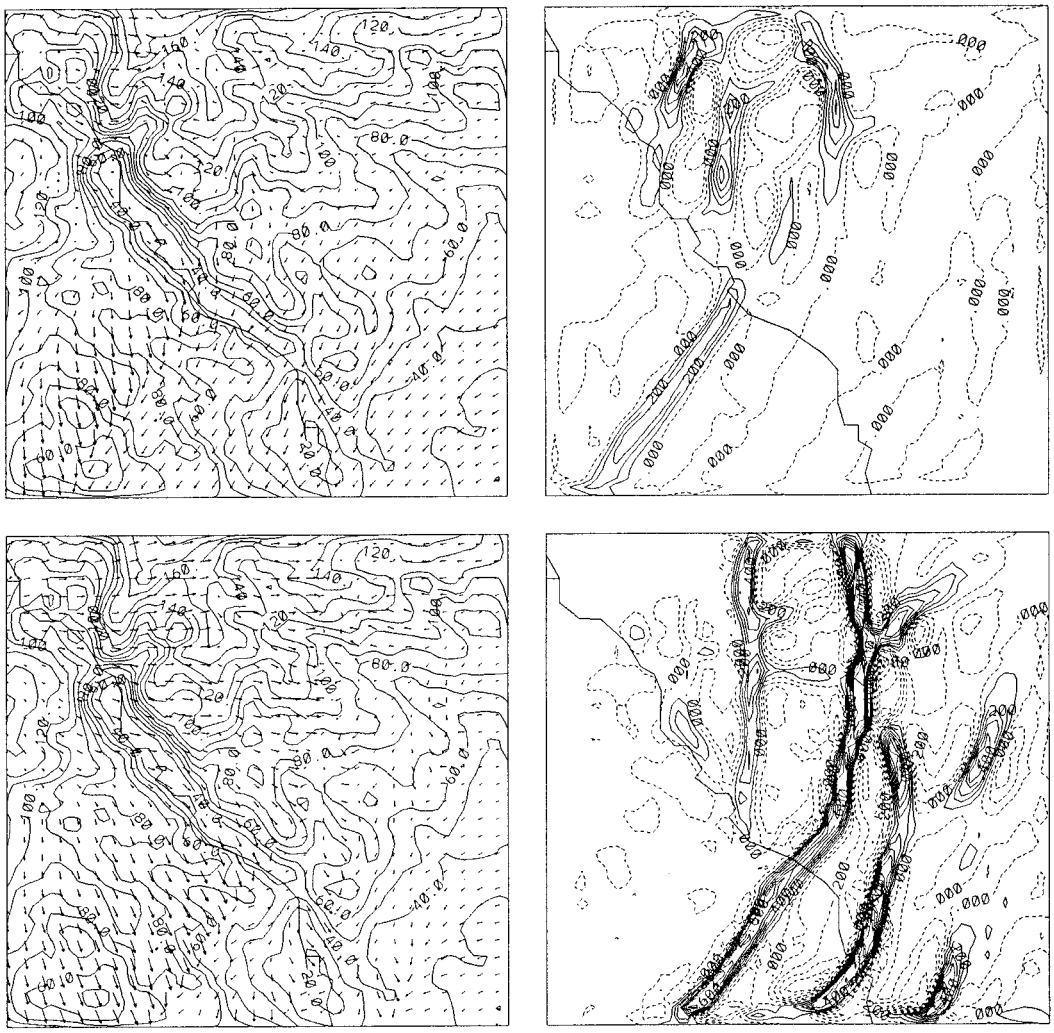

FIG. 4. Horizontal wind vectors (left panels) overlaid on the topography (contour interval 10 m) and vertical velocity field (right panels) ≈ 320 m above the surface for Case 1 (top panels, bare soil) and Case 2 (bottom panels, vegetation). Time is 1500 LST (Local Standard Time). All are Grid 3. The contour interval for the vertical velocity field is 10 cm/s.

moisture flux conveyances forming the dryline, and destabilizing the local air mass to deep convection; and (3) development of simulated deep dryline convection is sensitive to the assumed vegetative state of the ground surface.

These effects are even important with relatively strong winds. For this dryline case the surface layer winds were on the order of 10 m/s. While mesoscale circulations generated by heterogeneities in the vegetation pattern will become less if the prevailing wind is sufficiently strong, the moisture and heat fluxes to the atmosphere can be enhanced by the stronger winds as, for example, air cooled through transpiration and/or evaporation over one region travels over a warmer

←

PLATES 11–12. Plate 11 (top, parts a and b): Model output cloud and water vapor mixing ratio fields on the third nested grid (grid 4) at 21 GMT (Greenwich Mean Time) on 15 May 1991. The clouds are depicted by white surfaces with q_c = 0.01 g/kg, with the sun illuminating the clouds from the west. The vapor mixing ratio in the planetary boundary layer is depicted by the green surface with q_v = 8 g/kg. The tan surface is the ground. Areas formed by the intersection of clouds or the vapor field with lateral boundaries are flat surfaces, and visible ground implies $q_v < 8$ g/kg. The vertical axis is height, and the blue backplanes are the north and east sides of the grid domain. Plate 12 (bottom): Vegetation type interpolated to grid 3 (see Fig. 3). The classes are as follows: 1 cropland, 2 short grass, 3 evergreen needleleaf tree, 5 deciduous broadleaf tree, 10 irrigated cropland, 14 water, 18 mixed woodland.

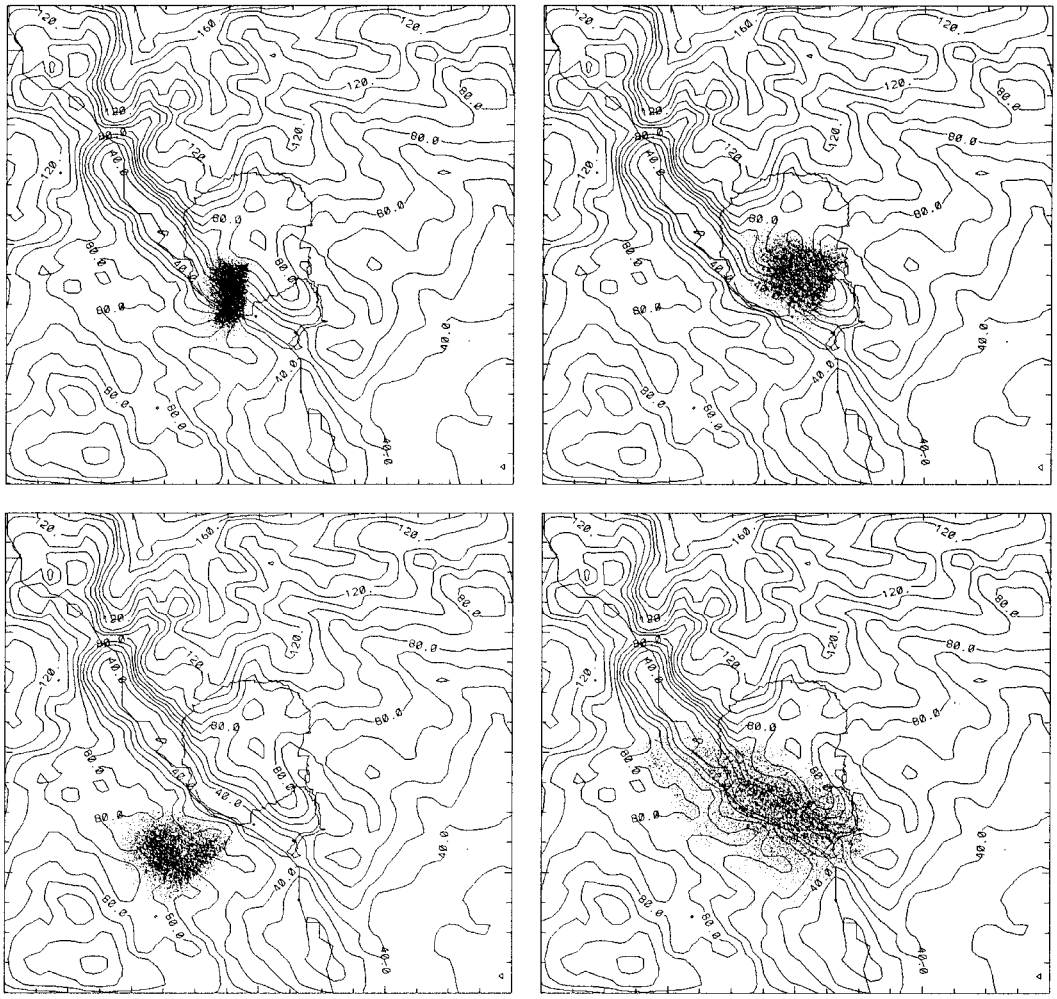

FIG. 5. A top view of particle positions 2 h after the start of the release at 1600 LST (Local Standard Time) (upper panels) and 4 h after the start of the release at 1800 LST (lower panels) for Case 1 (left panels) and Case 2 (right panels). Particles were released from near the center of the laboratory site.

surface area. The stronger fluxes, of course, are partially offset by reduced residence time over a location.

Use of the USGS vegetation data to study pollutant dispersion

When synoptic forcing is weak (as it often is in the southeast U.S. during the summer months when the weather is dominated by the Bermuda High), pollutant dispersion is largely controlled by locally generated mesoscale circulations such as sea breezes and mountain-valley circulations. Recent modeling studies have shown that variations in land cover can also generate local mesoscale circulations (Segal et al. 1988, Avissar and Pielke 1989). Here we have used the USGS vegetation data set to investigate the local mesoscale circulations generated by variable surface vegetation, and to study how these circulations affect pollutant dispersion around the Savannah River Laboratory site (SRL), which is located along the east bank of the Savannah River, ≈32 km south of Aiken, South Carolina. Previously it had been difficult to realistically assess the impacts of land use variations on local circulations and pollutant dispersion because high-resolution vegetation data sets were not available.

RAMS was used to simulate local mesoscale circulations around SRL. The model was run with a sponge lateral boundary condition that permits model-generated perturbations to exit the model domain, and not be reflected back in. A friction layer was used in the top eight model layers to absorb vertically propagating gravity waves. The model domain consisted of three nested grids, which are shown in Fig. 3. Each grid had 36 levels in the vertical, with a vertical grid spacing starting at 80 m near the surface, stretching up to 1 km at higher levels. Since thermally driven mesoscale circulations (such as those driven by variations in land cover) are strongest when synoptic forcing is weak, we chose to simulate a day when the weather

pattern over the southeastern United States was dominated by weak high pressure (24 May 1990). Two cases were run. The control case (Case 1) was initialized with bare soil. The second case (Case 2) was initialized with the same initial conditions as in Case 1, but the USGS vegetation data were used. The vegetation interpolated to grid 3 and converted to BATS classifications is shown in Plate 12. The SRL and state boundaries are shown in yellow. Both simulations were started at 0700 LST and ended 24 h later. Since thermally forced mesoscale circulations are strongest in the afternoon, results are shown for midafternoon unless otherwise stated. The horizontal and vertical velocities for grid 3 are shown in Fig. 4. Even in the absence of vegetation, local circulations are generated by terrain variations (top panels). There is a weak circulation extending from the southwest end of SRL to the southwest corner of the grid, and several smaller but more intense circulations to the north of the laboratory site. When vegetation is included, the circulations generated by topography are modified, and additional circulations are generated (bottom panels). The vertical velocity field shows one main circulation extending from the south of SRL, then northward along the east side of the laboratory site, and then to the north. The updrafts in this circulation are more intense than those found in Case 1. There is also a weaker circulation extending along the west side of the laboratory and to the north. Several smaller circulations can also be seen to the east of SRL.

To evaluate how these circulations affect pollutant dispersion, a Lagrangian Particle Model (McNider et al. 1988), which is driven by output from RAMS, was used. We chose to simulate a point release ≈40 m above the surface near the center of the laboratory site. Approximately 11 000 particles were released over a 30-min period beginning at 1400 LST. The particles were then traced for a period of 4 h.

Some of the results from the particle model runs are shown in Fig. 5. The particle positions 2 h after the start of the release for Case 1 and Case 2 are shown in the upper panels. In Case 1, the particles are advected to the southwest end of the laboratory and the plume does not disperse much horizontally. In Case 2 the plume is advected to the southeast and is entrained in the circulation along the eastern boundary of the laboratory. Four hours after the start of the release, the particles in Case 1 (bottom left panel) continue to be advected to the southeast and entrained into the weak circulation southwest of the laboratory site. In Case 2 (bottom right panel), the particles have been injected higher into the atmosphere by the strong mesoscale circulation along the eastern end of the laboratory site, and are spread out along the Savannah River Valley.

The model results shown here indicate that land use variations can have a significant impact on local atmospheric circulations and pollutant dispersion. The results also showed (although not discussed here) that the type of surface vegetative cover can affect the structure and evolution of the boundary layer, which could not only impact local pollutant dispersion, but also long-range transport.

Conclusions

These studies clearly demonstrate that landscape, including its spatial heterogeneity, has a substantial influence on the overlying atmosphere. Thus environmental policy-makers need to consider this feedback to weather and climate, rather than just assuming the atmosphere is an external factor to such issues as ecosystem management and water resource management. This feedback between the atmosphere and the land surface needs to be considered on all spatial scales from the plot scale to the global scale. This includes studies being performed at the Long-Term Ecological Research (LTER) sites that have been established throughout the United States. This paper also demonstrates the value of the USGS data in weather and climate simulations. We plan to continue this exploration as part of our USGS support, and through the related projects that critically depend on the USGS landscape information.

Acknowledgments

This research was supported by the United States Geological Survey, Department of the Interior under Assistance number 1434-94-A-1275, the National Aeronautics and Space Administration under Grant number NAG5-2078, The National Park Service through Contract number CA-1268-2-9004 TO-03, the National Science Foundation under Grant number ATM-9306754, Contract number 116 from the University of South Carolina, and Contract number UAH SUB93-183 from the University of Alabama. We thank Lou Steyaert and Tom Loveland for their continuing professional input to this work. A portion of this research was conducted while C. Ziegler was on a sabbatical leave to the NSSL/Mesoscale Research Division in Boulder, Colorado from 1 July 1992 to 31 July 1993. Initial fields were generated on the National Center for Atmospheric Research (NCAR) Cray-YMP (Shavano) under NSF Grant number ATM-8915265 to Colorado State University while some of the numerical simulations were performed on an IBM RS-6000 workstation at the National Severe Storms Laboratory. Robert Walko, Peter Olsson, and Jeff Copeland are gratefully acknowledged for assisting in the installation of CSU RAMS on Shavano and the NSSL IBM workstation. NCAR is sponsored by the National Science Foundation. Dallas McDonald is acknowledged for very effectively editing this paper.

Literature Cited

André, J.-C., P. Bougeault, J.-F. Mahfouf, P. Mascart, J. Noilhan, and J.-P. Pinty. 1989*a*. Impact of forests on mesoscale meteorology. Philosophical Transactions of the Royal Society of London **324**:407–422.

André, J.-C., J. P. Goutorbe, T. Schmugge, and A. Perrier. 1989*b*. HAPEX-MOBILHY: results from a large-scale field experiment. Pages 13–20 *in* A. Rango, editor. Remote sensing and large-scale global processes. International Association of Hydrological Sciences, Wallingford, United Kingdom.

Avissar, R., and F. Chen. 1993. Development and analysis of prognostic equations for mesoscale kinetic energy and mesoscale (subgrid-scale) fluxes for large-scale atmospheric models. Journal of Atmospheric Science **50**:3751–3774.

Avissar, R., and R. A. Pielke. 1989. A parameterization of heterogeneous land surfaces for atmospheric numerical models and its impact on regional meteorology. Monthly Weather Review **117**:2113–2136.

Balling, R. C., Jr. 1988. The climatic impact of a Sonoran vegetation discontinuity. Climatic Change **13**:99–109.

Beljaars, A. C. M., and A. A. M. Holtslag. 1991. Flux parameterization over land surfaces for atmospheric models. Journal of Applied Meteorology **30**:327–341.

Beljaars, A. C. M., P. Viterbo, M. J. Miller, and A. K. Betts. 1996. The anomalous rainfall over the US during July 1993: sensitivity to land surface parameterization. Monthly Weather Review **124**:362–383.

Betts, A. K., and A. C. M. Beljaars. 1993. Estimation of effective roughness length for heat and momentum from FIFE data. Atmospheric Research **30**:251–261.

Bolle, H.-J., et al. 1993. EFEDA: European Field Experiment in a Desertification threatened Area. Annales de Geophysique **11**:173–189.

Brown, J. F., T. R. Loveland, J. W. Merchant, B. C. Reed, and D. O. Ohlen. 1993. Using multi-source data in global land-cover characterization: concepts, requirements, and methods. Photogrammetric Engineering and Remote Sensing **59**:977–987.

Chang, J. T., and P. J. Wetzel. 1991. Effects of spatial variations of soil moisture and vegetation on the evolution of a prestorm environment: a case study. Monthly Weather Review **119**:1368–1390.

Chen, C., and W. R. Cotton. 1987. The physics of the marine stratocumulus-capped mixed layer. Journal of Atmospheric Science **44**:2951–2977.

Climate Analysis Center. 1993. Weekly climate bulletin, Number 93/32, Climate Analysis Center, Washington D.C., USA.

Copeland, J. H. 1995. Impact of soil moisture and vegetation distribution on July 1989 climate using a regional climate model. Dissertation. Atmospheric Science Department Paper Number 574, Colorado State University, Fort Collins, Colorado, USA.

Cotton, W. R., and R. A. Pielke. 1995. Human impacts on weather and climate. Geophysical Science Series. Volume 2. Cambridge University Press, New York, New York, USA.

Dalu, G. A., R. A. Pielke, R. Avissar, G. Kallos, M. Baldi, and A. Guerrini. 1991. Linear impact of thermal inhomogeneities on mesoscale atmospheric flow with zero synoptic wind. Annales de Geophysique **9**:641–647.

Dickinson, R. E., A. Henderson-Sellers, and P. J. Kennedy. 1993. Biosphere-Atmosphere Transfer Scheme (BATS) Version 1e as coupled to the NCAR Community Climate Model. Technical Report NCAR/TN-387+STR, National Center for Atmospheric Research, Boulder, Colorado, USA.

Dickinson, R. E., A. Henderson-Sellers, P. J. Kennedy, and M. F. Wilson. 1986. Biosphere-Atmosphere Transfer Scheme (BATS) for the NCAR Community Climate Model. Technical Report NCAR/TN-275+STR, National Center for Atmospheric Research, Boulder, Colorado, USA.

Doran, J. C., et al. 1992. The Boardman regional flux experiment. Bulletin of the American Meteorological Society **73**:1785–1795.

Eidenshink, J. C. 1992. The 1990 Conterminous U.S. AVHRR data set. Photogrammetric Engineering and Remote Sensing **58**:809–813.

Experiment Plan. 1993. Boreal Ecosystem-Atmosphere Study, July 1993, Version 1.0, 1–3. National Aeronautics and Space Administration, Goddard Space Flight Center. Greenbelt, Maryland, USA.

Gash, J. H. C., and W. J. Shuttleworth. 1991. Tropical deforestation: albedo and the surface-energy balance. Climatic Change **19**:123–133.

Gash, J. H. C., J. S. Wallace, C. R. Lloyd, A. J. Dolman, M. V. K. Sivakumar, and C. Renard. 1991. Measurements of evaporation from fallow Sahelian Savannah at the start of the dry season. Quarterly Journal of the Royal Meteorological Society **117**:749–760.

Guo, Y., and P. H. Schuepp. 1994. An analysis of the effect of local heat advection on evaporation over wet and dry surface strips. Journal of Climate **7**:641–652.

Hane, C. E., C. L. Ziegler, and H. B. Bluestein. 1993. Investigation of the dryline and convective storms initiated along the dryline. Bulletin of the American Meteorological Society **74**:2133–2145.

Lee, T. J. 1992. The impact of vegetation on the atmospheric boundary layer and convective storms. Dissertation. Department of Atmospheric Science, Colorado State University, Fort Collins, Colorado, USA.

Lee, T. J., and R. A. Pielke. 1996. GIS and atmospheric modeling: a case study. Pages 239–242 *in* M. F. Goodchild, L. T. Steyaert, B. O. Parks, C. Johnston, D. Maidment, M. Crane, and S. Glendinning, editors. GIS and environmental modeling: progress and research issues. GIS World Books, Fort Collins, Colorado, USA.

Lee, T. J., R. A. Pielke, T. G. F. Kittel, and J. F. Weaver. 1993. Atmospheric modeling and its spatial representation of land surface characteristics. Pages 108–122 *in* M. Goodchild, B. Parks, and L.T. Steyaert, editors. Environmental modeling with GIS. Oxford University Press, New York, New York, USA.

Louis, J. F. 1979. A parametric model of vertical eddy fluxes in the atmosphere. Boundary Layer Meteorology **17**:187–202.

Loveland, T. R., J. W. Merchant, D. O. Ohlen, and J. F. Brown. 1991. Development of a land-cover characteristics database for the conterminous U.S. Photogrammetric Engineering and Remote Sensing **57**:1453–1463.

Mahrt, L., and M. Ek. 1993. Spatial variability of turbulent fluxes and roughness lengths in HAPEX-MOBILHY. Boundary Layer Meteorology **65**:381–400.

Mahrt, L., J. I. McPherson, and R. Desjardins. 1994*a*. Observations of fluxes over heterogeneous surfaces. Boundary Layer Meteorology **67**:345–367.

Mahrt, L., J. Sun, D. Vickers, J. I. Macpherson, and J. R. Pederson. 1994*b*. Observations of fluxes and inland breezes over a heterogeneous surface. Journal of Atmospheric Science **51**:2484–2499.

Manqian, M., and J. Jinjun. 1993. A coupled model on land-atmosphere interactions—simulating the characteristics of the PBL over a heterogeneous surface. Boundary Layer Meteorology **66**:247–264.

McCumber, M. 1980. A numerical simulation of the influence of heat and moisture fluxes upon mesoscale circulations. Dissertation. University of Virginia, Charlottesville, Virginia, USA.

McNider, R. T., M. D. Moran, and R. A. Pielke. 1988. Influence of diurnal and inertial boundary layer oscillations on long-range dispersion. Atmospheric Environment **22**: 2445–2462.

Noilhan, J., J. C. André, P. Bougeault, J. Goutorbe, and P. Lacarrere. 1991. Some aspects of the HAPEX-MOBILHY programme: the data base and the modelling strategy. Surveys in Geophysics **12**:31–61.

Pielke, R. A., W. R. Cotton, R. L. Walko, C. J. Tremback, W. A. Lyons, L. D. Grasso, M. E. Nicholls, M. D. Moran, D. A. Wesley, T. J. Lee, and J. H. Copeland. 1992. A comprehensive meteorological modeling system—RAMS. Meteorology and Atmospheric Physics **49**:69–91.

Pielke, R. A., G. Dalu, J. S. Snook, T. J. Lee, and T. G. F.

Kittel. 1991. Nonlinear influence of mesoscale land use on weather and climate. Journal of Climate **4**:1053–1069.

Pielke, R. A., J. H. Rodriguez, J. L. Eastman, R. L. Walko, and R. A. Stocker. 1993. Influence of albedo variability in complex terrain on mesoscale systems. Journal of Climate **6**:1798–1806.

Pielke, R. A., and M. Uliasz. 1993. Influence of landscape variability on atmospheric dispersion. Journal of Air and Waste Management **43**:989–994.

Pielke, R. A., X. Zeng, T. J. Lee, and G. A. Dalu. 1996. Mesoscale fluxes over heterogeneous flat landscapes for use in larger scale models. Journal of Hydrology, *in press.*

Raupach, M. R. 1991. Vegetation-atmosphere interaction in homogeneous and heterogeneous terrain: some implications of mixed layer dynamics. Pages 105–120 *in* A. Henderson-Sellers and A. Pitman, editors. Vegetation and climate interactions in semi-arid regions. Kluwer, Dordrecht, The Netherlands.

Rhea, J. O. 1966. A study of thunderstorm formation along drylines. Journal of Applied Meteorology **5**:58–63.

Schädler, G., N. Kalthoff, and F. Fiedler. 1990. Validation of a model for heat, mass, and momentum exchange over vegetated surfaces using LOTREX 10E/HIBE88 data. Contributions to Atmospheric Physics **63**:85–100.

Schaefer, J. T. 1973. The motion and morphology of the dryline. NOAA Technical Memo **ERL NSSL-66** (National Technical Information Service, Number COM-74-10043).

Segal, M., and R. W. Arritt. 1992. Non-classical mesoscale circulations caused by surface sensible heat-flux gradients. Bulletin of the American Meteorology Society **73**:1593–1604.

Segal, M., R. Avissar, M. C. McCumber, and R. A. Pielke. 1988. Evaluation of vegetation effects on the generation and modification of mesoscale circulations. Journal of Atmospheric Science **45**:2268–2292.

Segal, M., W. Schreiber, G. Kallos, R. A. Pielke, J. R. Garratt, J. Weaver, A. Rodi, and J. Wilson. 1989. The impact of crop areas in northeast Colorado on midsummer mesoscale thermal circulations. Monthly Weather Review **117**:809–825.

Sellers, P. J., F. G. Hall, G. Asrar, D. E. Strebel, and R. E. Murphy. 1992. An overview of the First International Satellite Land Surface Climatology Project (ISLSCP) Field Experiment (FIFE). Journal of Geophysical Research **97**:18345–18371.

Shuttleworth, W. J. 1985. Daily variations of temperature and humidity within and above Amazonian forest. Weather **40**:102–108.

Smith, E. A., A. Y. Hsu, W. L. Crosson, R. T. Field, L. J. Fritschen, R. J. Gurney, E. T. Kanemasu, W. P. Kustas, D. Nie, W. J. Shuttleworth, J. B. Stewart, S. B. Verma, H. L. Weaver, and M. L. Wesley. 1992. Area-averaged surface fluxes and their time-space variability over the FIFE experimental domain. Paper Number 91JD03060. Journal of Geophysical Research **97**:18599–18622.

Tremback, C. J., and R. Kessler. 1985. A surface temperature and moisture parameterization for use in mesoscale numerical models. Seventh Conference on Numerical Weather Prediction, 17–20 June 1985, Montreal, Canada. American Meteorological Society, Boston, Massachusetts, USA.

Wallace, J. S., I. R. Wright, and J. B. Stewart. 1991. The Sahelian Energy Balance Experiment (SEBEX): ground based measurements and their potential for spatial extrapolation using satellite data. Advances in Space Research **11**:131–142.

Wetzel, P. J., and J.-T. Chang. 1988. Evapotranspiration from nonuniform surfaces. A first approach for short-term numerical weather prediction. Monthly Weather Review **116**:600–621.

Wood, E. F., D. P. Lettenmaier, and V. G. Zartarian. 1992. A land-surface hydrology parameterization with subgrid variability for general circulation models. Journal of Geophysical Research **97**:2717–2728.

Wright, I. R., J. H. C. Gash, H. R. Da Rocha, W. J. Shuttleworth, C. A. Nobre, G. T. Maitelli, C. A. G. P. Zamparoni, and P. R. A. Carvalho. 1992. Dry season micrometeorology of central Amazonian ranch-land. Quarterly Journal of the Royal Meteorological Society **118**:1083–1099.

Zeng, X., and R. A. Pielke. 1995. Further study on the predictability of landscape-induced atmospheric flow. Journal of Atmospheric Science **52**:1680–1698.

Ziegler, C. L., and C. E. Hane. 1993. An observational study of the dryline. Monthly Weather Review **1221**:1134–1151.

Ziegler, C. L., W. J. Martin, R. A. Pielke, and R. L. Walko. 1994. A modeling study of the dryline. Journal of Atmospheric Science **52**:263–285.